The following manuscript was written according to "**Recommendations for the Conduct, Reporting, Editing, and Publication of Scholarly Work in Medical Journals"**, December 2013 update, published by the International Committee of Medical Journal Editors and free accessible at http://www.icmje.org/.

LIST OF ABREVIATIONS:

ADC = Apparent Coefficient Diffusion

bIHCA = β-catenin-mutation plus Inflammatory Hepatocellular Adenoma

CNR = Constrat-to-noise

DW MRI = Diffusion-weighted Magnetic Resonance Imaging

Gd-EOB-DTPA = Gadoxetate Dissodium

HCA = Hepatocellular Adenoma

HCC = Hepatocellular carcinoma

HNF1A = Hepatocyte nuclear factor 1 α

IHCA = Inflammatory Hepatocellular Adenoma

MRI = Magnetic Resonance Imaging

OC = Oral contraceptives

ROI = Region of interest

SD = Standard Deviation

SI = Signal intensity

SNR = Signal-to-noise

Hepatocellular Adenomas: Characterization of Histological Subtypes Using Magnetic Resonance Imaging

Ana Cláudia Gemelgo, Célia Antunes, Filipe Caseiro Alves

Faculdade de Medicina da Universidade de Coimbra, Portugal

Clínica Universitária de Radiologia, Hospitais da Universidade de Coimbra, Portugal

Contact information:

Ana Cláudia Gemelgo Silva, address: Rua da Ribeirinha, nº 12, 5340-051, Bornes, Macedo de Cavaleiros, Portugal; telefone number: +351 916209427; e-mail address: gemelgoacs@hotmail.com

Number of figures: 5**; Number of graphics:** 3; **Number of Tables**: 1.

ABSTRACT

Purpose: identification of Magnetic Resonance Imaging (MRI) features specifically associated with each subtype of Hepatocellular adenoma (HCA); assessment of SNR (signal-to-noise), CNR (contrast-to-noise) and the Apparent Diffusion Coefficient (ADC) in dynamic MRI studies for each HCA subtype.

Materials and Methods: Fourteen patients (13 women, 1 man) with HCAs measuring ≥ 1 cm were evaluated retrospectively. Reference for standard diagnosis was obtained by immunohistochemistry data. A total of eighteen lesions were morphologically and dynamically studied in MRI (at 1.5 T). A contrasted-enhanced study was performed using Gadoxetate Dissodium (Gd-EOB-DTPA) with a breath-hold sequence with fat saturation. Two different regions of interest (ROIs) in the liver were analyzed to assess apparent diffusion coefficient (ADC) for Diffusion Weighted (DW) MRI with three *b*-values. Comparative analyses across groups were performed for SNR, CNR and ADC data.

Results: All HCAs were seen as hypervascular masses, characterized by heterogeneity in the Inflammatory and Steatotic groups. The Steatotic group had the higher wash-in and wash-out profile. Intra-lesional fat appears to be an important feature related to this type of HCAs. The DW MRI study showed no differences between groups.

Conclusion: The histological subtypes of HCAs have different imaging behavior which can be helpful to guide therapeutic choices. The ADC, however, proved unhelpful for this purpose. Limitations of the study prevented the conclusive analyses of the Beta-mutated adenomas. Future work will require the inclusion of more lesions.

Keywords: Hepatocellular adenomas, Histological subtypes of HCAs, MRI, Gd-EOB-DTPA, DW MRI, ADC

INTRODUCTION

Hepatocellular adenoma (HCA) is a rare tumor (incidence <0.004%) [1] that is mainly found in women of child-bearing age. In approximately 90% of all cases, HCAs are strongly related to current and recent oral contraceptives intake (OC) or others estrogens use. Non-OC-related causes of HCAs include familial insulin-dependent diabetes, Fanconi anaemia, β-thalassemia, glycogen storage diseases, and hormonal stimulation from other sources, for instance, anabolic steroid use by body builders, gynecological tumors, or pregnancy.[2]

HCAs are often asymptomatic. Right upper abdominal quadrant fullness or discomfort may be present due to mass effect. Typical clinical manifestations are acute abdominal pain with possible progression to hypotension and even death, due to spontaneous rupture or hemorrhage. Malignant transformation to hepatocellular carcinoma (HCC) is possible, but rare.[1, 2]

HCAs are typically solitary lesions (70 to 80%). Hepatic adenomatosis is a condition defined by the presence of 10 or more lesions, and is independent of gender or hormone therapy. HCAs vary in size from a few millimeters to several centimeters. The lesions are often in the right lobe of the liver. They are soft and smooth with large prominent blood vessels on the surface and within the tumor, with areas of hemorrhage and necrosis. There is usually no fibrous capsule; as a result, hemorrhage from an adenoma can freely extend into the liver.[1] Microscopically, adenomas are composed of a monoclonal mass of non-functional hepatocytes, with no portal areas nor bile ducts.[1]

A classification of HCA according to genotype and phenotype characteristics has been recently proposed.[2-7] Different molecular features associated with HCA have been described that define the following four main subgroups of lesions with close genotype-phenotype relationships: 1) inflammatory HCAs were defined by the presence of inflammatory infiltrates and by increased expression of inflammatory proteins in tumor hepatocytes (serum amyloid A

and C-reactive protein). Inflammatory HCAs represent 40 to 50% of all HCAs.[8, 9] 2) Hepatocyte nuclear factor-1α (HNF1A) gene mutated hepatocellular adenomas are the second most common subtype (30%–40%) of HCAs.[10] Non-functioning HNF1A protein leads to lipogenesis, hepatocellular proliferation and accumulation of intracellular fat, being represented by Steatotic adenomas as the end result. HNF1A inactivated HCAs are characterized by marked steatosis in the tumor hepatocytes.[8, 10] 3) The third group is related to catenin/cadherin-associated protein beta 1 (CTNNB1) mutations and activation of Wnt/ β-catenin pathway, and is responsible for about 10-15% of all HCAs.[2, 3, 7, 11] 4) A final group accounts for 10% to 25% of HCAs' cases and shows no specific genetic alterations; this group is therefore currently referred to as "unclassified".[2, 3]

The authors noted that adenomas associated with hepatocellular carcinoma (or having histologic features bordering on hepatocellular carcinoma) were observed almost exclusively in the β-catenin group, rarely in the HNF1A group, and never in inflammatory lesions. These observations suggest that adenomas with mutations in β-catenin may be at increased risk for malignant transformation.[12]

Since MRI is considered the most comprehensive and noninvasive imaging work-up for HCA diagnosis[13-15,] the purpose of this study is to identify MRI features specifically associated with each HCA subtype, correlating the MRI and histological findings. We aim to determine SNR (signal-to-noise), CNR (contrast-to-noise) and the Apparent Diffusion Coefficient (ADC) in dynamic MRI studies for each HCA subtype.

MATERIALS AND METHODS

Study design

This retrospective study included patients identified in the database of our institution for MR imaging reports who underwent MR imaging of the liver with both Diffusion Weighted

MRI (DWI MRI) study and Gadoxetate Dissodium (Gd-EOB-DTPA) enhanced imaging, between January 2009 and December 2013 and who had biopsy or surgical specimens confirming the diagnosis of HCA.

Approval by the ethical committee was waived attending to the retrospective nature of the study, assuring patient data confidentiality.

All cases were histologically proven and assessed by an experienced pathologist by immunohistochemistry techniques described previously.[8]

MR Imaging Technique

MR imaging was performed on a 1.5-T system (Symphony Class, Siemens, Erlangen, Germany). The routine MRI protocol included a breath-hold T1-weighted study with in-phase and out-of-phase sequences (TR, 100 ms; TE, 2.32/5.24 ms; flip angle, 70°; matrix, 256 × 180; slice thickness, 9 mm; intersection gap, 1,8 mm; field of view, 350 × 350 mm) and a respiratory-triggered T2-weighted FSE sequence (TR/TE, 1800/93 ms; flip angle, 150°; fat suppression, matrix, 384 × 264; slice thickness, 8 mm; intersection gap, 1,6 mm; field of view, 360 × 270 mm).

Dynamic imaging was performed using 3D T1-weighted GRE volumetric interpolated breath-hold sequence with fat selective prepulse (TR, 3.64; TE, 1.44; flip angle, 8°; matrix, 256 × 256; slice thickness 3.5; intersection gap 0.7mm; field of view, 400 x 400). Images were acquired before the administration of contrast agent (unenhanced phase) and 25–30 seconds (arterial phase), 70–90 seconds (portal venous phase), 3–5 minutes (equilibrium phase), and 20 minutes (hepatocyte phase) after i.v. bolus administration of Gd-EOB-DTPA at a dose of 0.025 mmol/kg of body weight followed by 20–30 mL saline flush. The injection rate used was 2 mL/s (for both contrast and saline flush). The optimal arterial phase was based on bolus tracking.

Diffusion-weighted images were acquired using an EPI sequence with fat suppression (TR/TE, 2300/70 ms; matrix, 204×160; slice thickness, 8 mm; intersection gap, 1,6mm; field of view, 380 × 380 mm; ≈ 2 min acquisition time). The gradient factors (b-values) were 0, 50 and 700 s/mm2. For shortening echo train length, integrated parallel imaging techniques (iPAT) were used and, for respiratory triggering, PACE (prospective acquisition correction) was implemented. Data was acquired during the end-expiratory phase.

ADC maps were calculated automatically from all diffusion weightings on a voxel-by-voxel basis and three images were generated: b = 0 s/mm^2; b= 50 s/mm^2, b= 700 s/mm^2 and the correspondent ADC map.

Image Analysis

The review of all MR images and previous exams was performed on a PACS workstation (SIENET Magic, v50, Siemens, 2004).

Analysis and measurements were made by a reader with three years of experience in abdominal MRI. In the presence of multiple lesions, all the lesions > 1cm were studied.

For all lesions, the following image features were noted by the radiologist: signal intensity on T1- and T2-weighted images (slightly hypointense, markedly hypointense, isointense, slightly hyperintense, or markedly hyperintense), presence of macroscopic hemorrhagic component (defined as focal T1-weighted hyperintense area), presence of necrotic or cystic component (defined as pronounced hyperintense signal on T2-weighted images), and the presence of fat within the lesion.

In order to assess the behavior of liver lesions with Gd-EOB-DTPA, we analyzed the images obtained prior to injection and during the dynamic study. Two regions of interest (ROI) of at least 1cm^2 at the level of the liver in the pre-contrast images were drawn: one inside the lesion and another in normal surrounding parenchyma (avoiding vessels and biliary ducts).

ROIs inside the lesion were placed in most homogeneous areas, avoiding areas of necrosis and hemorrhage. These same ROIs were then copied to the images obtained after administration of Gd-EOB-DTPA (in the arterial, portal, delayed and hepatospecific phases).

Background image noise was estimated placing circular ROIs of at least $10cm^2$ anteriorly to the right lobe of the liver, in extracorporeal position.

The contrast-to-noise ratio (CNR) of the lesions on 3D T1-GRE pre and post-contrast studies was calculated as (SIlesion – SIliver)/SDbackground, where SIliver is the signal intensity of the liver parenchyma.

The signal-to-noise ratio (SNR) of the lesions on 3D T1-GRE pre and post-contrast studies was calculated as SIlesion/SDbackground, where SIlesion is the signal intensity of lesion and SDbackground is the standard deviation of the signal intensities of the background noise.

A curve of SNR and CNR vs time was then calculated.

In order to assess the ADC of the different subtypes of HCAs, in the ADC map two ROIs of at least $1cm^2$ at the level of the liver in the pre-contrast images were drawn: one inside the lesion and another in normal surrounding parenchyma (avoiding vessels and biliary ducts). When the lesion was not well visualized on the ADC map, the T2-weighted image, the contrast enhanced T1-weighted images and the b50 images served as a roadmap for accurate ROI placement.

An ADC ratio was then calculated for each lesion as follows: (ADCLesion/ADCLiver), in which ADCLesion is the ADC of the lesions and ADCLiver is the ADC of the surrounding liver parenchyma.

Statistical analyses

All statistical analyses were performed using SPSS v17 (SPSS Inc, Chicago, IL). For statistical considerations, each lesion was taken as an independent subject by itself. This is defendable insofar as each lesion has characteristics that are of interest when taken individually, and within each patient the range of lesions is diverse, and do are the underlying conditions of normal-appearing surrounding liver.

Given the small number of subjects within each group, all testes were non-parametric, for any type of measurement. As the bIHCA group only had 2 subjects in it, this was not included in any inferential analyses, being, however, used within the descriptive analyses. For continuous variables, when comparing the 3 surviving groups, the Kruskal-Wallis test was used, with Mann-Whitney post-hoc tests when applicable, with Bonferroni correction.

For categorical data, the Fisher exact test was used. Intrinsic limitations of the study allowed us to only use 2 groups for these analyses (Steatotic and IHCA).

The continuous variables in this study were related to the SNR and CNR time changes of the scans as explained above. In order to extract a usable, sole metric for each subject, the mean slope of change was calculated over time, so as to evaluate and compare the behavior of each different HCA subtype towards the contrast agent.

RESULTS

The final analysis included a total of 14 patients (13 women and 1 man) and 18 HCAs.

Two patients had multiple lesions. One patient (the male one) had a previous clinical history of anabolic steroids intake for a period of time not known.

Among the series, the HCAs were divided in 4 groups: 1) Inflammatory group (IHCA) (n=7); 2) Steatotic group (n=3), which includes HNF1A mutated adenomas and histological

Steatotic adenomas when no mutation was possible to be confirmed; 3) β-catenin mutation group plus Inflammatory component (bIHCA) (n=2); 4) Unclassified group (n=6).

General Imaging features

Regarding the evaluation of signal intensity on T1-weighted images and T2-weighted images (***Graphic 1***), we found out that the IHCA group was mostly hypointense on T1-weighted images and hyperintense on T2-weighted images. A similar behavior was found in the Steatotic group for T2-weighted images. As for the bIHCA group, lesions were found to vary from iso to slightly hyperintense on T1-weighted images and isointense on T2-weighted images. The unclassified subtype revealed slightly hypo/isointensity on T1-weighted images and hyperintensity on T2-weighted images. No texture pattern seemed to be relevant in the histological HCAs' subtype differentiation, though ICHA and Steatotic groups appeared predominantly heterogeneous in T1 and T2-weighted images. The presence of capsule or pseudo-capsule, calcification and central scar could not be related to a specific subtype. Only one lesion, from the bIHCA group, had macroscopic hemorrhage.

Signal Intensity in Conventional MRI

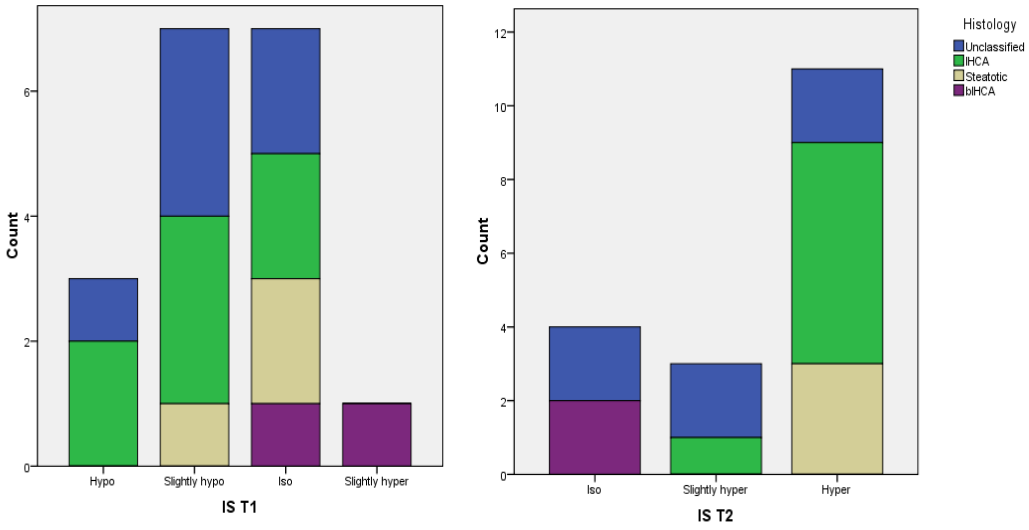

Graphic 1. Qualitative Signal Intensity for each group of adenomas in Conventional MRI for T1 and T2-weighted sequences.

Regarding intra-lesional fat, it seemed to be important in comparing IHCA and Steatotic lesions (G***raphic 2***.), once it is mostly related to the last group (p = 0.008 for Fisher's exact test). Two more adenomas with intra-lesional fat were found to belong to the Unclassified group. Due to its small sample size, bIHCA group could not be included in this evaluation.

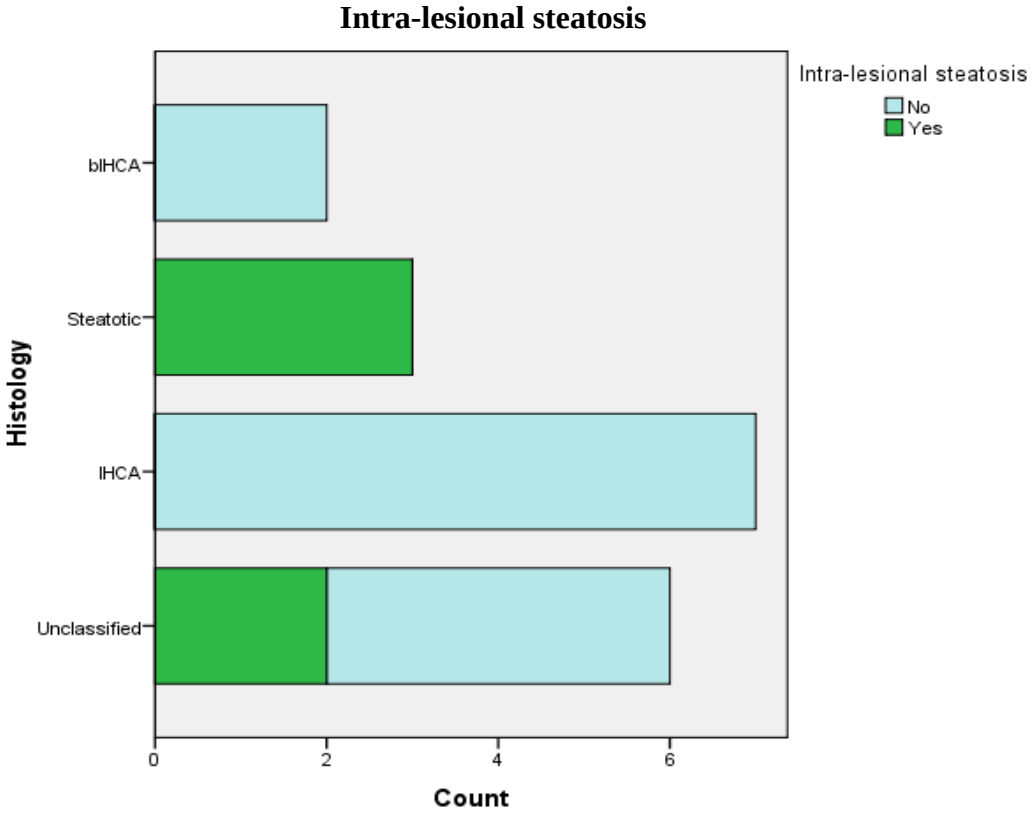

Graphic 2. Presence/absence of intra-lesional steatosis observed for each HCA subtype.

Gd-EOB-DTPA dynamic study

Regarding CNR analysis (***Graphic 3*** and ***Table 1***), the IHCA group (***Fig. 2***) demonstrated to have a higher wash-out rate, compared to normal surrounding liver (β = -3.148; p = 0.002), followed by the Steatotic group (β = -3.106; p = 0.035) (***Fig. 1***), and by the Unclassified group (β = -1.919; p < 0.001). CNR in delayed phase was not measured for one Steatotic lesion. As for the bIHCA group (***Fig. 3***), no significant difference to background liver

enhancement was found. When the Kruskal-Wallis test was applied to assess if there was a difference of wash-out rate between the first three groups, a value of p = 0.461 was found, suggesting similar rates.

In SNR analysis (***Graphic 3*** and ***Table 1***), we observed that the Steatotic group (***Fig.*** 1) was the one that showed a higher enhancement in arterial phase, compared to basaline images, followed by an marked drop-off of signal intensity in the remainder dynamic study (β = -0.726; p = 0.553). In the hepato-biliary phase the signal intensity of this subtype is almost equal as pre-contrast acquisition. SNR in delayed phase was not measured for one Steatotic lesion. Unclassified (β = 0.278; p = 0.811) and IHCA (β = 0.612; p = 0.549) (***Fig. 2***) subtypes reveal a similar behavior, characterized by the uptake of Gd-EOB-DTPA in arterial phase (although apparently less than the Steatotic group) that persists for the delayed phase, following by a slowly decrease in signal intensity in hepato-biliary phase. In the bIHCA group (***Fig. 3***), signal intensity does not change significantly during the dynamic Gd-EOB-DTPA study.

But yet, SNR analysis yielded no significant differences between the groups.

CNR and SNR behavior for Dynamic MRI

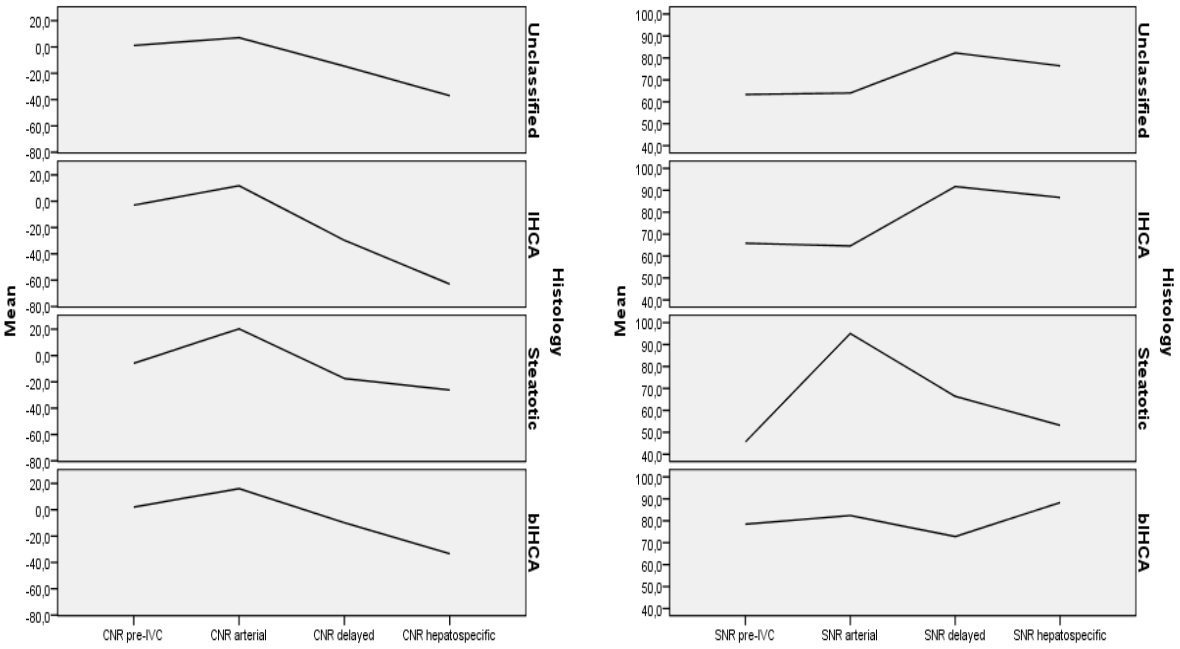

Graphic 3. Quantitative CNR and SNR behavior of each HCA group from pre-contrast to hepato-biliary phase.

Dynamic MRI study of a Steatotic HCA using Gd-EOB-DTPA

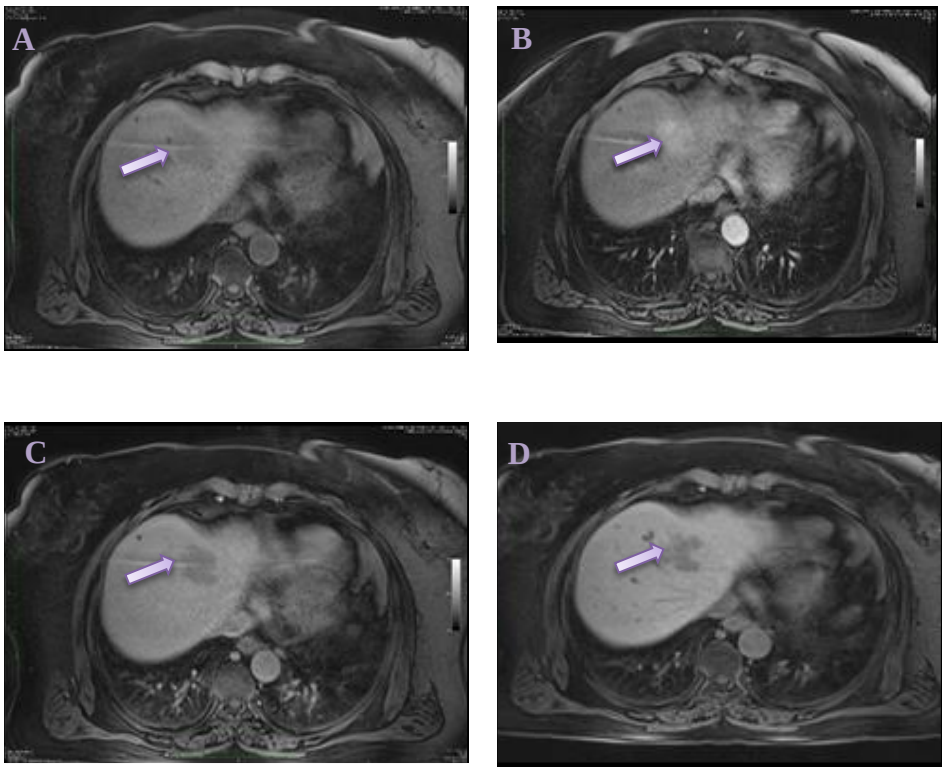

Fig. 1 – Dynamic MRI study of a Steatotic HCA in pre-IVC (A), arterial (B), delayed (C) and hepatospecific (D) phases. The lesion appears hypointense before contrast injection; the tumor is hypervascular in the arterial phase, and becomes hypointense in the delayed and hepatospecific phases.

Dynamic MRI study of a IHCA using Gd-EOB-DTPA

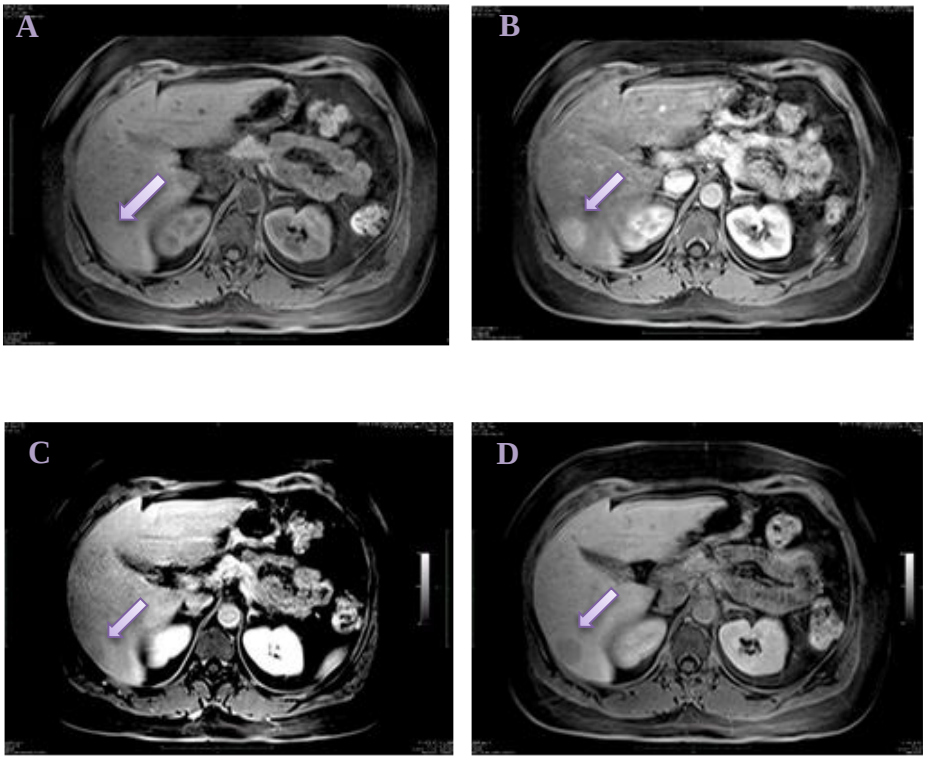

Fig. 2 – Dynamic MRI study of a IHCA in pre-IVC (A), arterial (B), delayed (C) and hepatospecific (D) phases. The lesion appears almost isointense before contrast injection; the tumor is hypervascular in the arterial phase, and shows washout in the delayed phase. In the hepatospecific phase it becomes hypointense compared to the surrounding parenchyma.

Dynamic MRI study of a bIHCA using Gd-EOB-DTPA

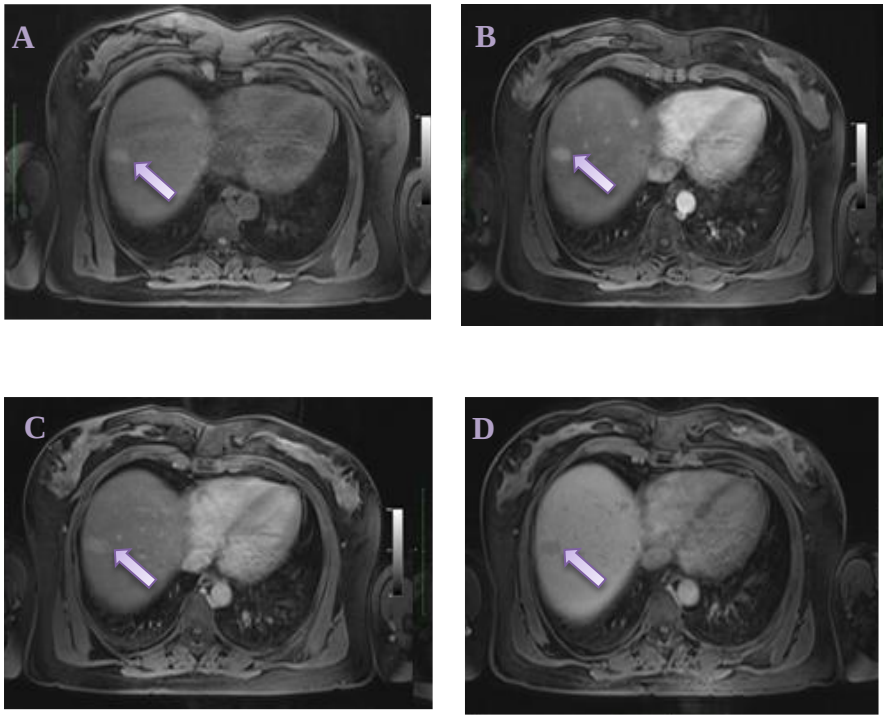

Fig. 3 – Dynamic MRI study of a bIHCA in pre-IVC (A), arterial (B), delayed (C) and hepatospecific (D) phases. The lesion appears slightly hyperintense before contrast injection and slightly enhances in the arterial phase, persisting in delayed phase. The tumor remains hypointense in the hepatospecific phase.

DWI MRI

The analysis of the ratio ADClesion / ADCliver was performed for each HCA subtype (***Table 1***). The values of this ratio were similar across all groups, with no statistical significance ($p = 0.905$). No cut-off value could be estimated (***Fig. 4*** and ***5***).

Steatotic HCA in Diffusion-weighted MRI

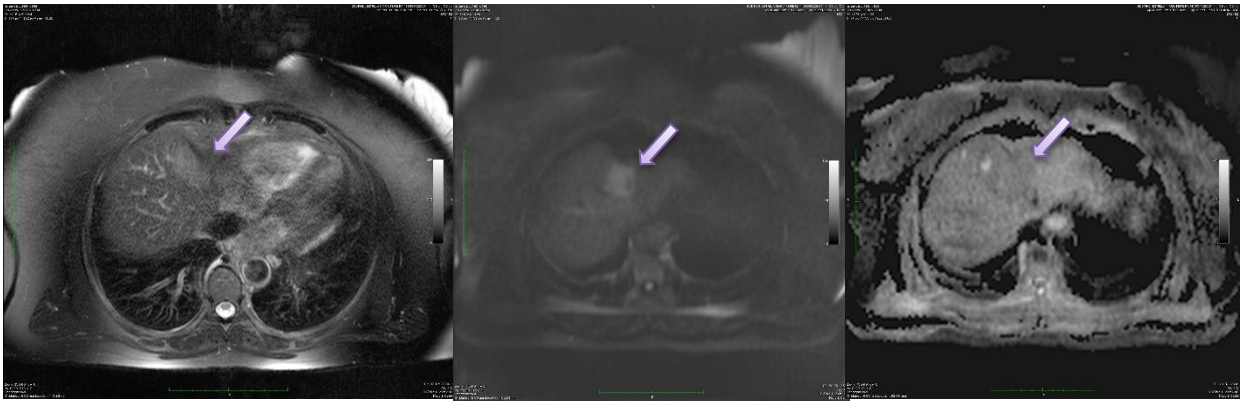

Fig. 4 **-** Diffusion-weighted MRI in a liver with a Steatotic HCA: (A) Fat-suppressed T2-weighted fast spin echo image shows a HCA located in the IV segment that is hyperintense to the liver; (B) in DW MRI with b = 700 sec/mm^2, the lesion shows slight hyperintensity compared with the background liver; (C) in the ADC map, the lesion has similar signal to the one presented in the liver.

IHCA in Diffusion-weighted MRI

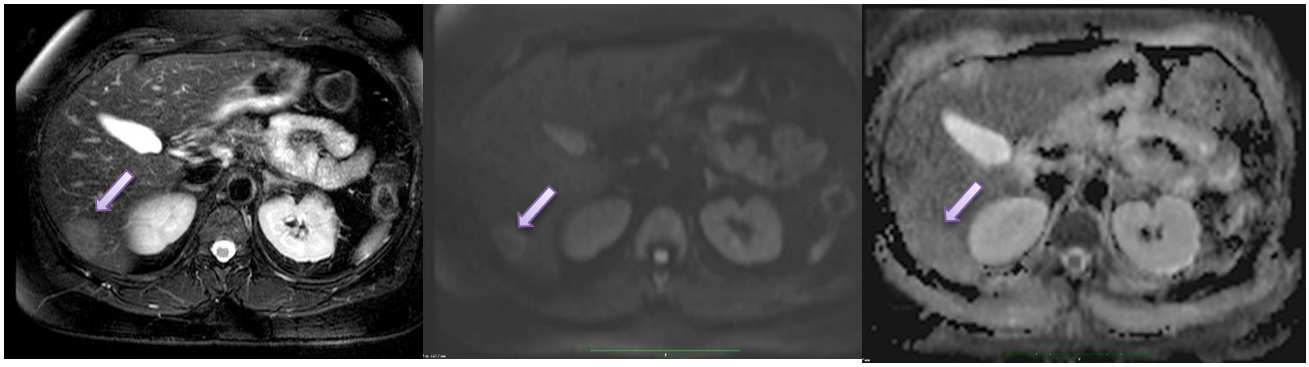

Fig. 5 **-** Diffusion-weighted MRI in a liver with a IHCA: (A) Fat-suppressed T2-weighted fast spin echo image shows a HCA located in the VI segment that is hyperintense to the liver; (B) in DW MRI with b = 700 sec/mm^2, the lesion is slightly hyperintense compared with the background liver; (C) in the ADC map, the lesion has a similar signal to the one presented in the liver.

CNR, SNR and ADC values measured for each histological subtype of HCAs

CNR (mean ± SD)	**Unclassified *(n=6)***	**Steatotic *(n=3)***	**IHCA *(n=7)***	**bIHCA *(n=2)***
pre-contrast	1.15 ± 8.55	-5.93 ± 1.80	-3.00 ± 10.10	2.10 ± 1.56
arterial phase	7.67 ± 12.73	16.90 ± 9.69	11.80 ± 5.70	16.10 ± 10.04
delayed phase	-14.57 ± 11.23	-17.45 ± 7.99*	-29.70 ± 26.91	-9,85 ± 21.85
hepato-biliary phase	-37.03± 18.60	-52.00 ± 44.77	-62.94 ± 47.17	-33.35 ± 55.08
SNR (mean ± SD)				
pre-contrast	63.33 ± 27.20	45.70 ± 16.00	65.83 ± 25.90	78.45 ± 17.32
arterial phase	63.98 ± 43.89	95.67 ± 9.61	64.61 ± 33.32	82.40 ± 11.88
delayed phase	82.28 ± 45.00	64.40 ± 39.74*	91.70 ± 40.73	72.80 ± 12.73
hepato-biliary phase	76.4 ± 39.04	72.90 ± 35.50	86.70 ± 43.23	88.30 ± 1.70
ADC (mean ±SD)				
ratio lesion / liver	**	1.29 ± 1.49	0.12 ± 1.09	1.17 ± 0.26

Table 1. The means and respective SD of CNR and SNR values for each HCA subtype group measured in pre-contrast, arterial, delayed and hepatospecific phases; and the mean of the ratio between ADC of the lesion and ADC of the liver.

* For the Steatotic group, one CNR and SNR value in the delayed phase was not measured.

**The Unclassified group was not included because three ADC values were not measured.

DISCUSSION AND CONCLUSION

From our results where the morphological and functional MR parameters of all HCA sub-types were analyzed, we have verified that Steatotic and IHCAs imaging profiles are in agreement to what has been described in literature.[3, 4], with IHCAs being mostly hypointense in T1 and hyperintense in FS T2-weighted sequences. Some heterogeneity was seen in both groups in both T1 and in T2 images, which may be explained by the frequent presence of sinusoidal dilatation and/or inflammatory infiltrates.[2] The signal intensity of the Steatotic HCAs group varied from an iso to hyperintense in T1 and T2-weighted images, which may be due as previously reported to their fatty or glycogen focal deposits.[2] Special attention must be drawn to the presence of intra-lesional fat as the most important and typical feature for characterizing Steatotic adenomas, since it was detected in all cases. No conclusion can be extracted for the bIHCAs' group, so it will not be mentioned.

Regarding dynamic study, all HCAs seem to be hypervascular masses with high enhancement in the arterial phase followed by wash-out in subsequent phases. IHCAs were seen as highly hypervascular adenomas, due to their arterial enhancement and little drop-off in delayed and hepatospecific phases. Steatotic adenomas, on the contrary, showed a diffuse drop-off pattern characterized by an intense arterial enhancement (high wash-in) that does not persist during subsequent phases (high wash-out). On hepato-biliary phase they were seen mostly as homogeneous and hypointense lesions. This behavior accounts for a typical imaging feature of Steatotic lesions.[3]

Concerning DW MRI study, no significant results were found, so the ADC value shall not be used to distinguish adenomas histological subtypes.

In summary, the results found in this study are comparable to the typical MRI behavior of HCAs already described [14, 18-20.], especially for IHCAs and Steatotic adenomas. All are focal lesions that have a higher SI in T2 than in T1-weighted images and behave as hypervascular

masses. Steatotic HCAs seem to be the most particular group of lesions, characterized by the presence of intra-lesional fat in morphological study, and an evident wash-in and wash-out patterns in dynamic MRI.

It must be underlined that this a pilot study, which shows that we have the right method to evaluate the different histological subtypes of HCAs. Further investigation in this field should be attained, though, and more lesions and subjects need to be studied. We find it very important to better profile HCAs imaging behavior, since the accurate diagnose has a major role in the final therapeutic approach of our patients.

ACKNOWLEDGMENTS:

The author would like to thank her supervisor Doctor and Professor Caseiro Alves for accepting to guide her in this project and her Master dissertation. This work could neither be possible without the support of Dr. Célia Antunes and Dr. Bruno Graça (Ph.D student), who were abundantly helpful and offered invaluable assistance. Thanks to Doctor João Pereira (Laboratório de Bioestatística e Imagem Médica, IBILI – FMUC, Portugal), as well, for his incredible attention and availability. The author is really graceful for all the help, preoccupation and dedication they paid to this project.

REFERENCES

1. Whitmer B. A., DO, Hepatocellular Adenomas, *Medscape Reference*, http://emedicine.medscape.com/article/1070205-overview (September 1, 2013), 2013.

2. Grazioli L., Olivetti L., Mazza G. and Bondioni M. P., MR Imaging of Hepatocellular Adenomas and Differential Diagnosis Dilemma, *International Journal of Hepatology*, vol. 2013, 20 pp., 2013.

3. Katabathina V. S., MD; Menias C. O., MD; Shanbhogue A. K. P., MD; Jagirdar J., MD; Paspulati R. M., MD, and Prasad S. R., MD, Genetics and Imaging of Hepatocellular Adenomas: 2011 Update, *RadioGraphics*, vol. 31, pp. 1529 – 1543, 2011.

4. Nault J. C., Bioulac-Sage P. and Zucman-Rossi J., Hepatocellular Benign Tumors – From Molecular Classification to Personalized Clinical Care, *Gastroenterology 2013*, vol. 144, pp. 888 – 902, 2013.

5. Ronot M., Bahrami S., Calderar J., Valla D. C., Bedossa P., Belghti J., Vilgrain V. and Paradis V., Hepatocellular Adenomas: Accuracy of Magnetic Resonance Imaging and Liver Biopsy in Subtype Classification, *Hepaology*, pp.1182 – 1190, 2011.

6. Borght S. V., Libbrecht L., Blokzijl H., Faber K. N., Moshage H., Aerts R., Steebergen W. V., Jansen P. L., Desmet V. J. and Roskams T. A., Diagnostic and

pathogeneic implications of the expression of hepatic transporters in focal lesions occurring in normal liver, *Journal of Pathology 2005*, vol. 207, pp. 471-482, 2005.

7. Zucman-Rossi J., Jeannot E., Nhieu JT., Scoazec JY., Guettier C., Rebouissou S., Bacq Y., Leteurtre E., Paradis V., Michalak S., Wendum D., Chiche L., Fabre M., Mellottee L., Laurent C., Partensky C., Castaing D., Zafrani ES., Laurent-Puig P., Balabaud C., Bioulac-Sage P., Genotype-phenotype correlation in hepatocellular adenoma: new classification and relationship with HCC, *Hepatology*. 2006; vol. 43(3), pp. 515.

8. Bioulac-Sage P, Rebouissou S, Thomas C, et al. Hepatocellular adenoma subtype classification using molecular markers and immunohistochemistry. *Hepatology* 2007; vol. 46, pp. 40–748.

9. Bioulac-Sage P,, Laumonier H,, Couchy G,, et al. Hepatocellular adenoma management and phenotypic classification: the Bordeaux experience. *Hepatology* 2009; vol. 50, pp. 481–489.

10. Bluteau O., Jeannot E., Bioulac-Sage P., et al. Biallelic inactivation of TCF1 in hepatic adenomas. Nat Genet 2002; vol. 32, pp. 312–315.

11. Chen YW., Jeng YM., Yeh SH., Chen PJ. P53 gene and Wnt signaling in benign neoplasms: beta-catenin mutations in hepatic adenoma but not in focal nodular hyperplasia. *Hepatology* 2002; vol. 36, pp. 927–935.

12. Agnello F., MD; Ronot M., MD; Valla D. C., MD; Sinkus R., PhD; Van Beers B. E., MD, PhD; Vilgrain V., MD, High-b-Value Diffusion-weighted MR Imaging of Benign Hepatocellular Lesions: Quantitative and Qualitative Analysis, *Radiology*, vol. 262, no 2, pp.511-519, 2012.

13. Chung KY., Mayo-Smith WW., Saini S., Rahmouni A., Golli M., Mathieu D., Hepatocellular adenoma: MR imaging features with pathologic correlation; *Roentgenol* 1995; vol.165, pp. 303–308.

14. Hussain SM., van den Bos IC., Dwarkasing RS., Kuiper JW., den Hollander J., Hepatocellular adenoma: findings at state-of-the-art magnetic resonance imaging, ultrasound, computed tomography and pathologic analysis; *EurRadiol* 2006; vol. 16, pp. 1873–1886.

15. Brancatelli G., Federle MP., Vullierme MP., Lagalla R., Midiri M., Vilgrain V. CT and MR imaging evaluation of hepatic adenoma; *Comput Assist Tomogr* 2006; vol. 30, pp. 745–750.

16. Dijkstra H., Baron P., Kappert P., Oudkerk M., Sujens P. E., Effects of microperfusion in hepatic diffusion weighted imaging, *Eur Radio 2012*, vol. 22, pp. 891-899, 2011.

17. Denecke T., Steffen G. I., Agarwal S., Seehofer D., Krôncke T., Hänninem E. L., Kramme I. B., Neuhaus P., Saini S., Hamm B. and Gieser C.,

Appearance of hepatocellular adenomas on gadoxetic-acid enhancement MRI, *Eur Radiol,* vol. 22, pp. 1769-1775, 2011**.**

18. Huppertz A., Balzer T., Blakeborough A., Breure J., Giovagnoni A., Heinz-Peer G., Laniado M., Mandrefi R. M., Mathieu D. G., Mueller D., Reimer P., Robinson P. J., Strotzer M., Taupitz M. and Vogl T. J., Improved Detection of Focal Liver Lesions at MR Imaging: Multicenter Comparison of Gadoxetic Acid–enhanced MR, *Radiology,* vol. 230, pp. 266-275, 2004.

19. Dogan Y., Soylu A., Kilickesmez O., Demirtas T., Kilichesmez K. O., Dogan S. N., Eren G., Sevindir I., Yasar N., Poturoglu S., Sonmez K., The Value of Hepatic Diffusion-weighted MR Imaging in Demostrating Hepatic Congestion Secondary to Pulmonary Hypertension, *Cardiovascular Ultrasound 2010,* 12 pp., 2010.

20. Quayyum A., Diffusion-weighted Imaging in Abdomen and Pelvis: Concepts and Applications, *RadioGraphics,* vol. 29, pp. 1797-1810, 2009.